Including Dynamic Line Rating Into the Optimal Planning of Distributed Energy Resources

Kateryna Morozovska, *Member, IEEE*, Miguel Heleno, *Member, IEEE*, Alan Valenzuela Meza, and Patrik Hilber, *Senior Member, IEEE*

***Abstract*—Dynamic line rating (DLR) is an emerging technology that can remove strict power transmission constraints and potentially reduce investment costs in new generation technologies in a microgrid. By implementing dynamic rating into distributed generation sizing and placement problem, it is possible to reduce the investment costs on new distributed energy resources by achieving improved optimal power flow results as compared to planning without considering DLR. This paper explores the possibility of complementing a model for optimal siting and placement of the distributed energy resources in a microgrid with the dynamic line rating. Implementation of DLR has shown a decrease in investment costs as well as a reduced number of installed generators as opposed to the solution without DLR implementation.**

***Index Terms*—Microgrid design, sizing and placement of generation, optimal power flow, dynamic line rating.**

I. Introduction

DYNAMIC line rating is a method of smarter line operation, which uses information on real-time weather parameters to unlock hidden line capacity. This unlocked capacity allows to remove network contingencies and achieve more efficient power flow [1], [2], [3], [4]. There are several studies which have explored the possibility of using dynamic line rating for power dispatch optimization in transmission and sub-transmission grids [1], [5], [6], [7]. Additionally, a possibility to combine dynamic line rating with a dynamic rating of power transformers for day-ahead optimal dispatch planning is explored in [8]. The potential to reduce the cost of microgrid operation under security constraints after the introduction of dynamic line rating is studied in [9].

Manuscript received October 25, 2020; revised February 23, 2021 and July 10, 2021; accepted August 16, 2021. Date of publication August 31, 2021; date of current version October 21, 2021. This work was supported in part by Ericsson EC, in part by SweGRIDS, in part by Swedish Energy Agency, and in part by Energiforsk AB Wind Research Program for Project Sponsorship. Paper no. TSG-01592-2020. *(Corresponding author: Kateryna Morozovska.)*

Kateryna Morozovska was with the Grid Integration Group, Lawrence Berkeley National Laboratory, Berkeley, CA 94720 USA. He is now with the Department of Electromagnetic Engineering, School of Electrical Engineering and Computer Science, KTH Royal Institute of Technology, 10044 Stockholm, Sweden (e-mail: kmor@kth.se).

Miguel Heleno and Alan Valenzuela Meza are with Lawrence Berkeley National Laboratory, Grid Integration Group, Berkeley, CA 94720 USA.

Patrik Hilber is with the School of Electrical Engineering, KTH Royal Institute of Technology, 10044 Stockholm, Sweden.

Color versions of one or more figures in this article are available at https://doi.org/10.1109/TSG.2021.3109130.

Digital Object Identifier 10.1109/TSG.2021.3109130

Several studies have shown improved optimal power dispatch after adding DLR to the system operation; however, little information is available in the literature on the benefits of planning the grids with dynamic rating, in particular, when solving long-term investment planning problems. Reinforcing capacities of the lines can remove some of the system's constraints, which in return can change an optimal planning solution, by creating new pathways for optimal power flow. Having power transfer limits dynamically adjusted, depending on the weather conditions, can decrease the number of required generators and the load curtailment.

Microgrids are locally connected group of loads, storage units and generation resources that should be able to operate both independently and as a part of a larger grid. A variety of optimization tools has been developed to plan DERs in remote communities, often operated as medium voltage (MV) microgrids. When communities are spread across larger territories, the power flow between the long-distance nodes becomes critical due to increase in power losses and additional limitations on the grid voltages and power line loading constraints. This type of grid planning problems is named siting and sizing of Distributed Energy Resources (DERs), and is, typically, formulated as a mixed-integer linear programming (MILP) optimization problem [10], [11]. In most cases, methods addressing siting and sizing of DERs optimize the portfolio and location of generation and storage units to meet load demand of the community [12], [13]. However, little attention has been brought to maximize also the cost-effectiveness of components responsible for power delivery, such as power lines.

On one hand [9] shows the DLR economic benefits on microgrid scheduling problem, however, these benefits are not being captured in the DER planning and microgrids design phase [10], [11], which is an important literature gap we are aiming to address. This paper proposes an addition to the model described in [10], which would allow using dynamic line capacity limits and gives the potential for more cost-effective sizing and placement of new DERs.

The usual practice is to have line transfer capacity constrained by the maximum current $I^{max} = 1p.u.$, however, dynamic rating allows to set maximum current above the rated value $I^{max}_{DLR} >= 1p.u.$ at each time step, depending on the weather conditions. The maximum current of DLR application is dependent on the temperature of the line; therefore the line power flow in this model is constrained by the maximum allowable line temperature for specified in the grid requirements, and line power flow becomes a function of ambient conditions.

The resulting model provides a more cost-effective solution for siting and sizing of DERs problem and better utilization of existing power lines, which results in more sustainable planning and utilization of assets. The proposed solution also evaluates a possibility for connecting the additional load to the network and evaluates the potential impact of the increase in load demand and electricity price. This novel approach to grid planning does not only reduce the cost of investment and operation but has a potential for improving the security of supply and opening additional opportunities for connecting new loads to the system. Together with that, loading electrical components closer to their maximum limits results in better utilization of existing infrastructure and requires fewer material resources and at the same time improves the overall environmental impact of the solution.

II. Methodology

The methodology describes the theory behind DLR application and also provides a detailed description of how DLR is integrated into the MILP model for optimal design of multi-energy microgrids [10].

A. Dynamic Line Rating

The ability of the power line to handle higher capacities is highly dependent on its heat balance (1) [14], [15]. Two mechanisms are mainly responsible for the heating of the line: a flow of electric current and line resistance, named Joule heating, $P_J = I^2R$ and absorption of electromagnetic waves from solar radiation, P_S [14], [15]. Cooling of the line is governed by convection and conduction, P_{conv} as well as emission of electromagnetic waves from the surface of the line to the surrounding media named radiation, P_{rad} [14], [15]. Traditionally, the current-carrying capacity of the line is a constant limit. Line's ampacity limit is constrained to be below the highest possible ampacity for the worst-case ambient conditions, such as high ambient temperatures and low wind speeds. The worst-case ambient conditions in terms of line's heat balance are high ambient temperatures and wind speeds below 1 m/s. Extreme weather has a negative impact on the line's cooling; however, the probability of occurrence of extreme weather is significantly low [16], [17], [18], [19].

Therefore, if the cooling of the line is sufficient, it often creates a possibility of transporting higher capacity using the same line. Steady-state conductor's heat balance as a function of conductor temperature and current is presented in (1).

$$P_J\left(I, T_{avg}\right) + P_s = P_{conv}(T_s) + P_{rad}(T_s) \tag{1}$$

where I is the current passing through the line, $[A]$; T_s is the temperature at the surface of overhead conductor, $[K]$; T_{avg} is the average temperature across conductor's cross-sectional area, which is a mean value of surface temperature T_s and core temperature T_c, $T_{avg} = (T_s + T_c)/2$, $[K]$.

Since Joule heating is a function of the line's current, this current can be expressed as a function of the line's surface temperature as shown in (2) and (3).

$$P_J(I, T_s, T_c) + P_s - P_{conv}(T_s) - P_{rad}(T_s) = 0 \tag{2}$$

$$I_{DLR} = \sqrt{\frac{P_{conv}(T_s) + P_{rad}(T_s) - P_s}{R(T_s, T_c)}} \tag{3}$$

It has to be noted that current temperature relationship is highly non-linear, and it becomes challenging to integrate dynamic line rating into the linear programming models. However, it is possible to express maximum allowable line ampacity at time t by using standard temperature limitations; when standard ratings are estimated, they are designed to constrain maximum conductor surface temperature to be within certain limit from grid regulations. By replacing the surface temperature of conductor T_s in (2) and (3) with the maximum allowable conductor's surface temperature T_s^{max} the relation for maximum allowable current ampacity (4) is obtained. Maximum allowable current ampacity of the line I_{DLR}^{max} is later used in optimization model formulation as an upper limit for line's current between each pair of nodes at each time step.

$$I_{DLR}^{max} = \sqrt{\frac{P_{conv}\left(T_s^{max}\right) + P_{rad}\left(T_s^{max}\right) - P_s}{R\left(T_s^{max}, T_c\right)}} \tag{4}$$

An overhead line can be approximated as a cylinder - temperature gradient in circular cross-sections is different from plane surfaces. Some studies argue on the importance of accounting the radial temperature difference [8], [14], [15]. However, the radial temperature difference is not taken into account in this study, since the focus is given to long-term planning, not a dispatch planning, where temperature gradient is more important for the safety of operation.

B. Optimization Model Formulation

The objective of the optimization model is to minimize the total investment and operation costs of the studied microgrid. The objective function (5) consists of the investment and Operation & Maintenance (O&M) costs for continuous technology (PV); total cost of electricity generation and purchase as well as possible revenue from export of excessive electricity.

$$\begin{aligned} C^{tot} = & \sum_n \left(C^{PV_{fix}} pur_n^{PV} + C^{PV_{var}} cap_n^{PV}\right) Ann^{PV} \\ & + \sum_n \left(C^{ST_{fix}} pur_n^{ST} + C^{ST_{var}} cap_n^{ST}\right) Ann^{ST} \\ & + \sum_{n,t} \left(Gen_{n,t} C^{PV_{O\&M}}\right) + \sum_{n,t} \left(chrg_{n,t} C^{ST_{Util}}\right) \\ & + \sum_{n,t} \left(UtPur_{n,t} C^{Pur}\right) - \sum_{n,t} \left(UtExp_{n,t} C^{Exp}\right) \\ & + \sum_{n,t} \left(LdCur_{n,t} \cdot C_n^{ENS}\right) \end{aligned} \tag{5}$$

where C^{tot} are total costs of microgrid's investment and operation, [\$]; $C^{PV_{fix}}/C^{ST_{fix}}$ are fixed costs for installing PV's/storage at the node n, [\$]; pur_n^{PV}/pur_n^{ST} is a binary decision variable, which specifies if there is a generation/storage installed at the node n; $C^{PV_{var}}/C^{ST_{var}}$ are variable costs for PV/storage operation, which depend on the maximum installed capacity, [$/kW]; cap_n^{PV}/cap_n^{ST} is the installed PV/storage capacity at node n, [kW]; Ann^{PV}/Ann^{ST} is the annuity rate for PV/storage; $Gen_{n,t}$ is the output of electricity generation from PV at the node n and time t, [kWh]; $C^{PV_{O\&M}}$ are variable annual operation and maintenance costs for PV technology depending on the amount of production, [$/kWh]; $chrg_{n,t}$ is the charge of the battery storage at the node n at time t, [kWh]; $C^{ST_{Util}}$ are the costs of utilization of the battery storage, [$/kWh]; $UtPur_{n,t}$ is the amount of electricity purchase from the utility at each node n at each time step t, [kW]; C_t^{Pur} is electricity price for electricity import at time t, [$/kWh]; $UtExp_{n,t}$ is the amount of electricity exported to the utility at each node n at each time step t, [kW]; C_t^{Exp} is electricity price for electricity export at time t, [$/kWh]; $LdCur_{n,t}$ is the amount of energy not supplied at node n time t, [kW]; C_n^{ENS} is the price for shedding load demand at node n, [$/kWh].

Equality constraints that ensure electricity balance are specified in (6) - (11). Equation (6) denotes that active power at node n is a sum of utility purchase and generation at a node minus utility export and load demand met for each node n. Equation (7) relates reactive power at each node except utility to the active power at that node and power factor.

$$S_{base} \cdot Pg_{n,t} = UtPur_{n,t} - UtExp_{n,t} + Gen_{n,t} - - \left(Ld_{n,t} - LdCur_{n,t}\right) - chrg_{n,t} + dischrg_{n,t} \tag{6}$$

$$Qg_{n,t} = Pg_{n,t} \cdot tan(acos(\phi)), \ for\ n \neq S \tag{7}$$

$$Vr_{n,t} = V0 + \frac{1}{V0} \sum_{n' \neq N} \left(Zr_{n,n'} Pg_{n',t} + Zi_{n,n'} Qg_{n',t}\right), \quad for\ n \neq S \tag{8}$$

$$Vi_{n,t} = \frac{1}{V0} \sum_{n' \neq N} \left(Zi_{n,n'} Pg_{n',t} - Zr_{n,n'} Qg_{n',t}\right), \quad for\ n \neq S \tag{9}$$

$$Vr_{n,t} = V0, \ for\ n = S \tag{10}$$

$$Vi_{n,t} = 0, \ for\ n = S \tag{11}$$

where S_{base} is base power, [kW]; $Pg_{n,t}$ is active power at node n at time t, [$p.u.$]; $Ld_{n,t}$ is the input parameter for load demand at the node n at time t, [kWh]; $dischrg_{n,t}$ is the amount of power discharge from the battery storage, [kWh]; $Qg_{n,t}$ is reactive power at each node, which is not a slack node, [$p.u.$]; S is used to denote slack bus; ϕ is power factor; $Vr_{n,t}$, $Vi_{n,t}$ are real and imaginary voltages at node n at time t respectively, [$p.u.$]; $V0$ is slack bus voltage, [$p.u.$]; $Zr_{n,n'}$, $Zi_{n,n'}$ are real and imaginary components of Zbus matrix between respective pair of nodes n-n', [$p.u.$]

Equation (6) represents the energy balance of the microgrid at the point of common coupling with the main grid. Equation (7) assumes a constant power factor and keeps a linear relationship between active and reactive power. Equations (8)-(11) present an approximation for the real and imaginary components of the voltage, considering the same assumptions stated in [1]. These bus voltage equations require introducing additional limits for ensuring that voltage magnitudes remain within acceptable minimum and maximum thresholds. A linear approximation is adopted from [20] and

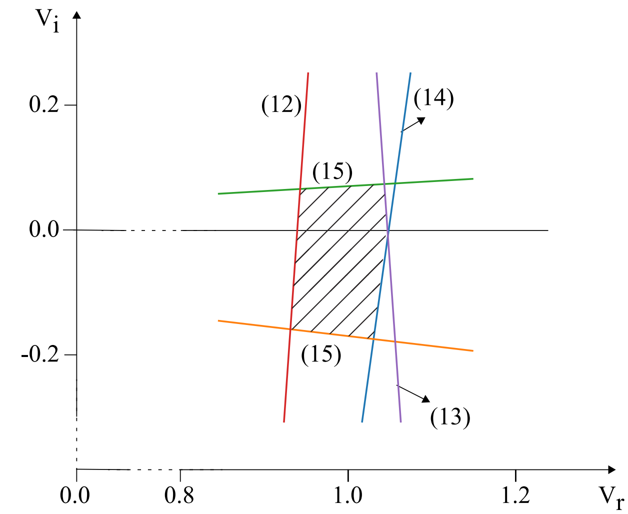

Fig. 1. Linear approximation of voltage constraints.

defined in (12), (13) and (15). However, (14) is formulated in a different manner in this manuscript to capture the behavior depicted in Fig. 1.

$$Vi_{n,t} \leq \frac{sin\overline{\theta} - sin\underline{\theta}}{cos\overline{\theta} - cos\underline{\theta}} \left(Vr_{n,t} - \underline{V} \cdot cos\underline{\theta}\right) + \underline{V} \cdot sin\underline{\theta} \tag{12}$$

$$Vi_{n,t} \leq \frac{sin\overline{\theta}}{cos\overline{\theta} - 1} \left(Vr_{n,t} - \overline{V}\right) \tag{13}$$

$$Vi_{n,t} \geq \frac{sin\underline{\theta}}{cos\underline{\theta} - 1} \left(Vr_{n,t} - \overline{V}\right) \tag{14}$$

$$Vr_{n,t} \cdot tan\underline{\theta} \leq Vi_{n,t} \leq Vr_{n,t} \cdot tan\overline{\theta} \tag{15}$$

where $\overline{V}$ and $\underline{V}$ are maximum and minimum acceptable voltage magnitudes, [$p.u.$]; $\overline{\theta}$ and $\underline{\theta}$ are maximum and minimum acceptable voltage angles, [rad].

A critical variable, which influences optimal placement and sizing of generators in the system is the minimization of the active and reactive power losses. Active and reactive power losses are defined both in terms of total active and reactive power injection respectively in (16)-(17) and square value of current multiplied by resistance and reactance respectively in (18)-(19).

$$\sum_n Pg_{n,t} = Ploss_t, \ for\ n = S \tag{16}$$

$$\sum_n Qg_{n,t} = Qloss_t, \ for\ n = S \tag{17}$$

$$Ploss_t = \frac{1}{2} \cdot \sum_{n,n'} R_{n,n'} \cdot \left(Ir_{n,n',t}^2 + Ii_{n,n',t}^2\right) \approx \frac{1}{2} \cdot \sum_{n,n'} R_{n,n'} \cdot \left(Ir_{n,n',t}^{Sq} + Ii_{n,n',t}^{Sq}\right) \tag{18}$$

$$Qloss_t = \frac{1}{2} \cdot \sum_{n,n'} X_{n,n'} \cdot \left(Ir_{n,n',t}^2 + Ii_{n,n',t}^2\right) \approx \frac{1}{2} \cdot \sum_{n,n'} X_{n,n'} \cdot \left(Ir_{n,n',t}^{Sq} + Ii_{n,n',t}^{Sq}\right) \tag{19}$$

where $Ploss_t$, $Qloss_t$ are total active and reactive power losses at time t respectively, $[p.u.]$; $R_{n,n'}$, $X_{n,n'}$ are resistance and reactance of the line between respective pair of nodes n-n', $[p.u.]$; $Ir_{n,n'}$, $Ii_{n,n'}$ are real and imaginary current of the line between busses n and n' respectively, $[p.u.]$; $Ir^{Sq}_{n,n',t}$, $Ii^{Sq}_{n,n',t}$ are approximated real and imaginary line current values between nodes n and n' respectively, $[p.u.]$

The first step for calculating approximated square values of real and imaginary current $Ir^{Sq}_{n,n',t}$, $Ii^{Sq}_{n,n',t}$ is to express real and imaginary components of the current $Ir_{n,n',t}$, $Ii_{n,n',t}$ in Cartesian coordinates as shown in (20) and (21) respectively.

$$Ir_{n,n',t} = -Yr_{n,n'} \cdot \left(Vr_{n,t} - Vr_{n',t}\right) + Yi_{n,n'} \cdot \left(Vi_{n,t} - Vi_{n',t}\right) \tag{20}$$

$$Ii_{n,n',t} = -Yi_{n,n'} \cdot \left(Vr_{n,t} - Vr_{n',t}\right) - Yr_{n,n'} \cdot \left(Vi_{n,t} - Vi_{n',t}\right) \tag{21}$$

where $Yr_{n,n',t}$, $Yi_{n,n',t}$ are real and imaginary terms of the bus admittance matrix, $[p.u.]$

Square values of real and imaginary current are obtained from a series of inequality constraints (22)-(25), where (22) and (23) approximate positive and negative values of the square value of real current from real current $Ir_{n,n',t}$ of the line and (24), (25) approximate positive and negative values of the square value of imaginary current from imaginary current $Ii_{n,n',t}$ of the line.

$$Ir^{Sq}_{n,n',t} \geq (v \cdot \Delta Ir)^2 + (2v-1) \cdot \Delta Ir \times \left(Ir_{n,n',t} - v \cdot \Delta Ir\right), v \in 1, \ldots, Nv \tag{22}$$

$$Ir^{Sq}_{n,n',t} \geq (v \cdot \Delta Ir)^2 - (2v-1) \cdot \Delta Ir \times \left(Ir_{n,n',t} + v \cdot \Delta Ir\right), v \in 1, \ldots, Nv \tag{23}$$

$$Ii^{Sq}_{n,n',t} \geq (v \cdot \Delta Ii)^2 + (2v-1) \cdot \Delta Ii \times \left(Ii_{n,n',t} - v \cdot \Delta Ii\right), v \in 1, \ldots, Nv \tag{24}$$

$$Ii^{Sq}_{n,n',t} \geq (v \cdot \Delta Ii)^2 - (2v-1) \cdot \Delta Ii \times \left(Ii_{n,n',t} + v \cdot \Delta Ii\right), v \in 1, \ldots, Nv \tag{25}$$

where Nv is the number of segments for the linear approximation of square value of the current magnitude; v is the number of the piece-wise segment for the linear approximation of square value of the current magnitude; ΔIr, ΔIi are calculated from the maximum expected value of the current magnitude divided by the number of segments Nv, $[p.u.]$

Values of ΔIr and ΔIi for the network with no DLR are calculated by division of current rating of the line $I^{max}_{n,n',t}$ by the number of segments Nv. In the original model [10] all the lines are assumed to be of the same size, therefore, having the same rating, however, in real-case scenarios lines in the system are often different and might have different rating. Taking this into account we propose to replace ΔIr and ΔIi components in equations (22)-(25) with $\Delta Ir_{n,n'}$ and $\Delta Ii_{n,n'}$ respectively. $\Delta Ir_{n,n'}$ and $\Delta Ii_{n,n'}$ for the system with constant rating limits are calculated by (26).

$$\Delta Ir_{n,n'} = \Delta Ii_{n,n'} = \frac{I^{max}_{n,n'}}{Nv}, [p.u.] \tag{26}$$

For the system with DLR applied the values of ΔIr and ΔIi are obtained by dividing maximum possible variable rating of the line $max(I^{DLR}_{n,n'})$ by the number of segments Nv as in ((27)).

$$\Delta Ir^{DLR}_{n,n'} = \Delta Ii^{DLR}_{n,n'} = \frac{max\left(I^{DLR}_{n,n'}\right)}{Nv}, [p.u.] \tag{27}$$

The maximum possible value of dynamic rating current can be restricted by the operator to ensure the safe operation and limiting mechanical damage to the conductor; in this model we assume $max(I^{DLR}_{n,n'}) = 1.6$ $p.u.$ and $max(I^{DLR}_{n,n'}) = 1.8$ $p.u.$ depending on the type of conductor. It has to be mentioned that the maximum allowable current at each time step is always the upper limit for the line current, value of $max(I^{DLR}_{n,n'})$ is only used to approximate square values of real and imaginary parts of the current magnitude. The number of segments Nv for the DLR model should be increased compared to the static rating model.

The ampacity constraints are enforced in (28) and (29) for static rating and dynamic rating models respectively.

$$Ir^{Sq}_{n,n',t} + Ii^{Sq}_{n,n',t} \leq I^{max}_{n,n'} \tag{28}$$

$$Ir^{Sq}_{n,n',t} + Ii^{Sq}_{n,n',t} \leq I^{DLR}_{n,n',t} \tag{29}$$

where $I^{DLR}_{n,n',t}$ is a maximum allowable line current at time t obtained from equation (3).

The purchase and export from/to the utility are modelled using constraints (30)-(31) and (32)-(33) respectively. The slack bus is assumed to be connected to the utility. In this model, energy purchase or exported from or to the utility can only be made at the slack node, although, this constraint can be adjusted depending on the system outline.

$$UtPur_{n,t} \leq psb_{n,t} \cdot M, \text{ } for \text{ } n = S \tag{30}$$

$$UtPur_{n,t} = 0, \text{ } for \text{ } n \neq S \tag{31}$$

$$UtExp_{n,t} \leq \left(1 - psb_{n,t}\right) \cdot \overline{UtExp}, \text{ } for \text{ } n = S \tag{32}$$

$$UtExp_{n,t} = 0, \text{ } for \text{ } n \neq S \tag{33}$$

where $psb_{n,t}$ is a binary decision variable for deciding if electricity is to be purchased from the utility or exported to the utility; $\overline{UtExp}$ is the maximum amount of energy that can be exported to the utility, $[kW]$.

Amount of solar generation at the node n is limited by the amount of maximum installed capacity cap^{PV}_n and by the purchase decision for installing PV pur^{PV}_n at that node and changes hourly depending on the solar production efficiency $SolarGen_{n,t}$ as shown in (34)-(35).

$$cap^{PV}_n \leq pur^{PV}_n \cdot M \tag{34}$$

$$Gen_{n,t} \leq cap^{PV}_n \cdot SolarGen_{n,t} \tag{35}$$

where M is a very large number.

The maximum installed storage capacity at the node n is constrained using (36). Maximum charge/discharge at the time t is regulated by constraints (37)-(40). State of charge of the battery is defined by inequality constraint (41) and equality constraint (42).

$$cap^{ST}_n \leq pur^{ST}_n \cdot M \tag{36}$$

$$chrg_{n,t} \leq cap^{ST}_n \cdot \overline{PCr} \tag{37}$$

$$dischrg_{n,t} \leq cap^{ST}_n \cdot \overline{PCr} \tag{38}$$

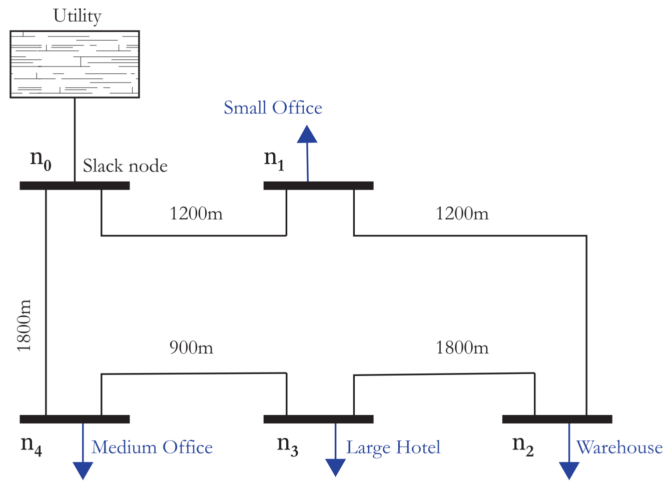

Fig. 2. Electrical network of microgrid used in the case study.

$$chrg_{n,t} \leq \alpha_{n,t} \cdot M \tag{39}$$

$$dischrg_{n,t} \leq \left(1 - \alpha_{n,t}\right) \cdot M \tag{40}$$

$$\underline{SOC} \cdot cap_n^{ST} \leq SOC_{n,t} \leq cap_n^{ST} \tag{41}$$

$$SOC_{n,t} = SOC_{n,t-1} + chrg_{n,t} \cdot \eta^{chrg} - \frac{dischrg_{n,t}}{\eta^{dischrg}} \tag{42}$$

where $\overline{PCr}$ is the maximum battery power/capacity ratio; $\alpha_{n,t}$ is a binary variable which defines if storage is in state of charge or discharge at the node n at time t; $\underline{SOC}$ is the battery minimum state-of-charge, $[kW]$; $SOC_{n,t}$ is the battery state-of-charge at the node n at time t, $[kW]$; η^{chrg} and $\eta^{dischrg}$ are battery charge and discharge efficiencies respectively.

III. Case Study

The optimization model formulation described in the previous section is applied to a following case study and results comparison between solutions with and without DLR are being presented in Section IV.

Case study is performed on 12 kV microgrid, which is presented in Fig. 2. Microgrid case is originally adopted from [10] but resized to fit the physical properties of the medium-voltage network and equipped with corresponding conductors for further dynamic line rating studies.

The microgrid is assumed to be located in Northern California near the San Francisco Bay Area. The weather data, used in this analysis, is a statistical representation of a typical meteorological year (TMY) for Northern California. The normalized PV production is derived from radiation data taken the TMY3 database [21]. Load profiles are taken from the DOE prototypical building database [22] for the same TMY location. Load demand at each node is distributed according to the type of consumer; typical weekday load demand for each consumer is shown in Fig. 3.

Given the TMY weather data and physical properties of chosen conductors, the real-time ampacity of lines was calculated as shown in Fig. 4. Maximum allowable conductor rating (limited to 1.6 $p.u.$), which is used in optimization model to limit Ir^{Sq} and Ii^{Sq} in (29) is also shown in Fig. 4.

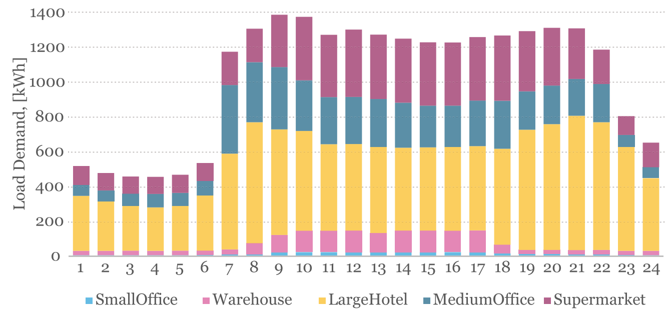

Fig. 3. Load demand distribution between different consumers during typical weekday.

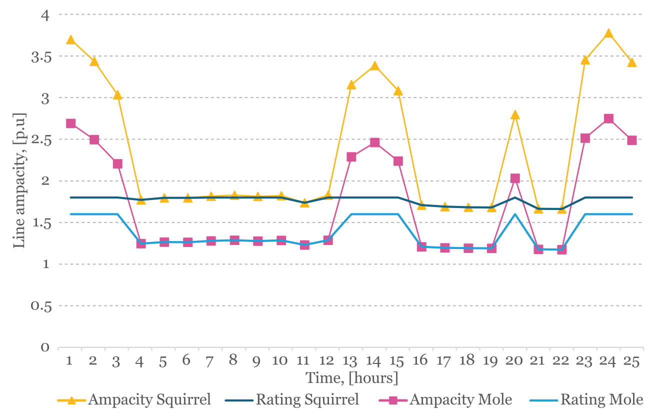

Fig. 4. Calculated line ampacity and maximal allowable ratings of the power lines from Table I for a selected weekday in 2018.

TABLE I
Parameters of Overhead Conductors in Figure 2

From node	To node	Line type	R, Ω/km	X, Ω/km	R_{tot}, Ω	D, mm	$\overline{I}$, $[A]$
1	2	Squirrel	1.39	0.331	1.67	6.33	77
1	5	Squirrel	1.39	0.331	2.51	6.33	77
2	3	Mole	2.78	0.342	3.37	4.50	48
3	4	Mole	2.78	0.342	5,00	4.50	48
4	5	Mole	2.78	0.342	2.50	4.50	48

Alternation between line sizes is also introduced. Table I shows conductor specification for each node. Table I also depicts maximum current carrying capacity (static rating) I_{max} in A for each conductor, assuming maximum allowable conductor temperature $T_s^{max} = 75\ °C$. Using the parameters of conductors from Table I and the conductor's current temperature relationship (4) [14], the real-time capacity limit for each line is calculated.

Storage technology is assumed to be Lithium-Ion battery; cost parameters of battery storage for residential area are presented in Table II [10], [23]. Cost parameters for solar and grid operation are taken for the state of California [24], [25] and are also presented in Table II.

First case study is performed on the grid presented in Fig. 2 with and without DLR. For studying the sensitivity of the model to the input parameters a comparison between Standard Line Rating (SLR) case and DLR case is performed for results

TABLE II
COST PARAMETERS INPUT DATA

Storage			PV & Grid data		
Parameter	Value	Units	Parameter	Value	Units
$C^{ST_{var}}$	300	$[\$/kWh]$	$C^{PV_{var}}$	2060	$[\$/kW]$
$C^{ST_{fix}}$	1	$[\$]$	$C^{PV_{fix}}$	1	$[\$]$
Ann^{ST}	0.117	–	Ann^{PV}	0.067	–
$C^{ST_{Util}}$	0.12	$[\$/kWh]$	$C^{PV_{O\&M}}$	0.10	$[\$/kWh]$
η^{chrg}	0.9	–	C^{Pur}	0.1979	$[\$/kWh]$
$\eta^{dischrg}$	0.9	–	C^{Exp}	0.056	$[\$/kWh]$

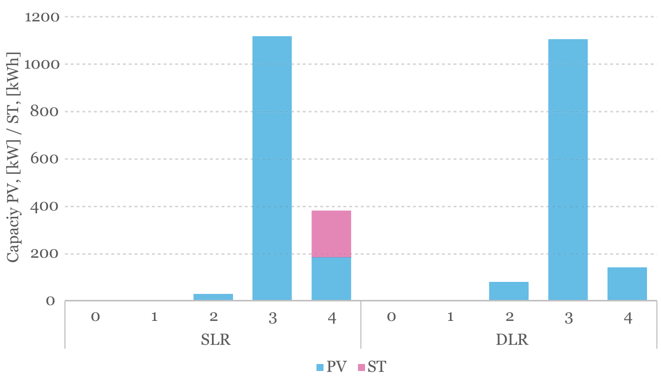

Fig. 5. Comparison between SLR and DLR solutions.

after assuming variability in electricity price and increase in power demand. Afterwards, an additional load "Supermarket" is connected to the bus $n2$ for comparison between methods.

IV. RESULTS

A MILP problem is solved with Gurobi solver [26] for one year with hourly time-steps. The total investment costs for the installation of new generators and storage units have been adjusted using the annuity rate to represent yearly cost impact.

A. Base Case

The comparison between investment solutions with and without DLR application is presented in Fig. 5 with more detailed solution presented in Table III. It is important to note that after dynamic rating application it is no longer optimal to invest in battery storage. The authors would argue that due to less constrained capacity limits on the power lines it becomes more profitable to invest in more solar generation and compensate for the hours with no production with utility purchase. Savings on the electricity storage allow to lower need in investment and total cost of yearly power supply as shown in Table IV.

B. Effect of Change in Electricity Price on Planning Solution

Different levels of changes in electricity price have been introduced in the model. Fig. 6 shows differences in PV and Storage capacity needed for SLR and DLR depending on the change in electricity price. Optimal solution for DLR does not include battery storage in the analyzed electricity price range.

TABLE III
SITING AND SIZING SOLUTION FOR EACH NODE FOR SLR AND DLR

SLR			DLR		
Type	Node	Size	Type	Node	Size
PV, $[kW]$	2	29	PV, $[kW]$	2	80
PV, $[kW]$	3	1120	PV, $[kW]$	3	1107
PV, $[kW]$	4	186	PV, $[kW]$	4	141
Storage, $[kWh]$	4	197			

TABLE IV
ANNUALIZED DER INVESTMENT COSTS & TOTAL YEARLY UTILITY COSTS

Cost type	SLR	DLR
Utility, [k$]	1179	1181
PV, [k$]	185	184
ST, [k$]	6	0
Total, [k$]	**1371**	**1365**

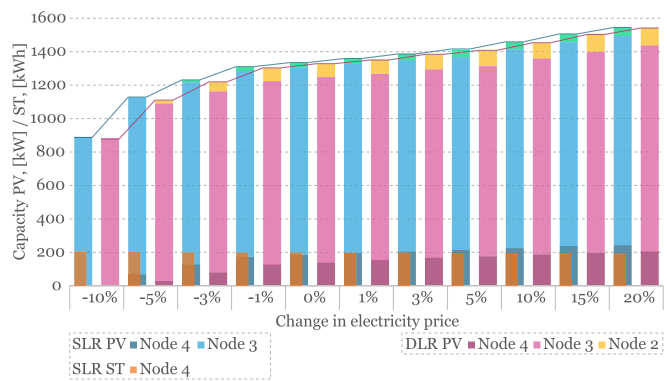

Fig. 6. Impact of the electricity price on the siting and sizing solution.

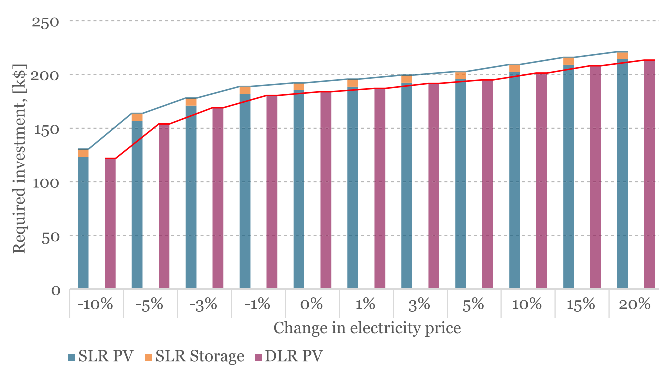

Fig. 7. Impact of the electricity price on the yearly investment in DERs.

For both SLR and DLR cases, it becomes more profitable to invest in more local generation resources with increase in electricity price and less profitable if the price drops. Fig. 7 is the representation of annualized investment costs in DERs depending on change in electricity price from utility and Fig. 8 shows total yearly costs of supply. The cost analysis shows that main contribution to the difference in needed investment between SLR and DLR cases is associated with battery storage. The DLR will allow to increase the energy consumption from the grid and, therefore, avoid the battery investments. However,

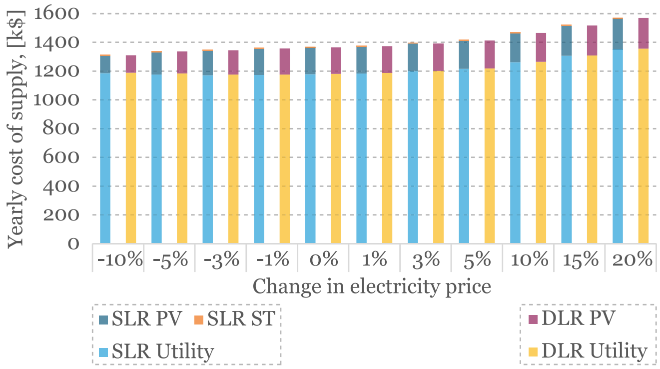

Fig. 8. Impact of the electricity price on the total yearly cost of electricity supply.

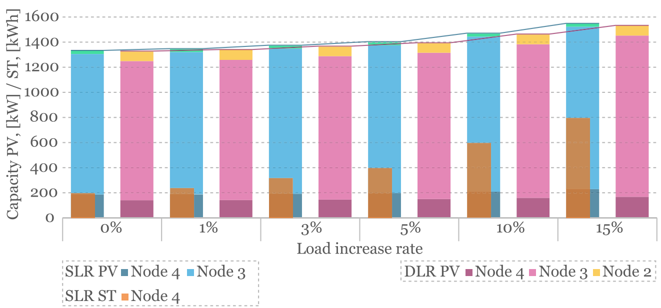

Fig. 9. Impact of the load increase on the decision of PV and Storage placement.

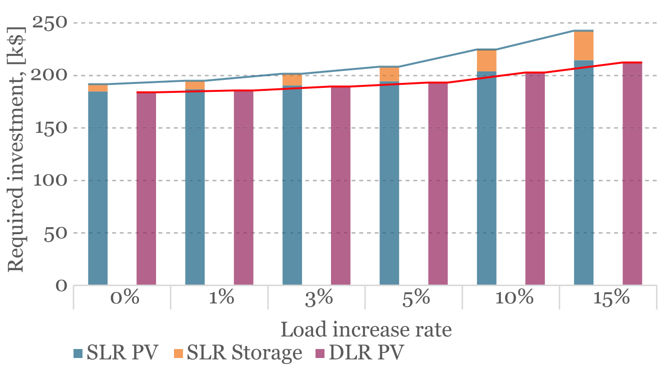

Fig. 10. Impact of the change in the load demand price on the yearly investment in DER.

the electricity price does not show significant limitations with both DLR and SLR following a slow upwards trend.

C. Impact of Load Increase on the Planning Solution

Total global energy demand is often projected to increase in the future, therefore it is important to analyse the sensitivity of the result to the increase in the load. Fig. 9 shows projected change in siting and sizing solution for PV with increase in the load demand for SLR and DLR. The upwards trend in the PV need is similar for SLR and DLR, with DLR always requiring lower capacity, however, SLR requires significant investment in energy storage to be able to supply the load. Although, unlike the study on change of electricity price, the load increase has more significant impact on the solution, as shown in Fig. 10 and Fig. 11 need in energy storage contributes to significant change in needed investment for SLR case. DLR scenario appears to be more economically robust to increase in load demand. A possibility of connecting additional load to one of the nodes has also been explored. When an additional load "Supermarket" is connected to the node $n2$, siting and sizing model without dynamic rating requires 20% more capacity than a DLR solution as can be seen from Table V. Table VI is a comparison between total costs of the base case and after adding the "Supermarket".

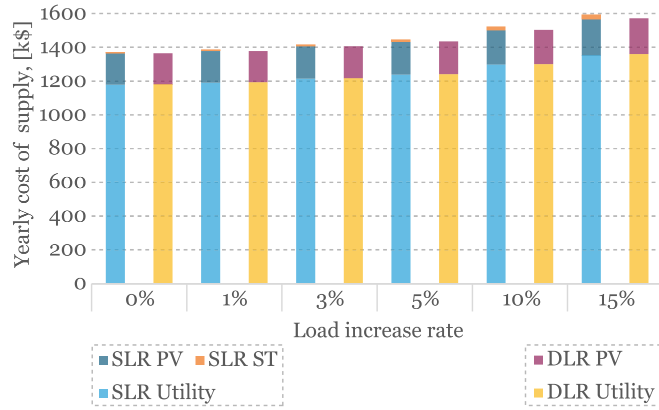

Fig. 11. Impact of the change in the load demand price on the total yearly cost of electricity supply.

TABLE V
RESULTING PURCHASE OF TECHNOLOGY AFTER ADDING "SUPERMARKET" LOAD AT THE NODE $n2$

SLR			DLR		
Type	Node	Size	Type	Node	Size
PV, $[kW]$	2	826	PV, $[kW]$	2	831
PV, $[kW]$	3	1072	PV, $[kW]$	3	1066
PV, $[kW]$	4	71	PV, $[kW]$	4	53
Storage, $[kWh]$	4	544			

TABLE VI
ANNUALIZED INVESTMENT COSTS FOR DERS AND TOTAL YEARLY UTILITY COSTS AFTER ADDING "SUPERMARKET" AT THE NODE $n2$

Cost type	with "Supermarket"		Base case	
	SLR	DLR	SLR	DLR
Utility, [k$]	1542	1551	1179	1181
PV, [k$]	273	270	185	184
ST, [k$]	19	0	6	0
Total, [k$]	**1834**	**1821**	**1371**	**1365**

V. CONCLUSION

Dynamic line rating has shown to significantly impact sizing and placement decision for DERs in microgrid. After application of dynamic rating to the grid, the number of installed PV panels and storage unit decreases, since the unlocked line limits allow for better distribution of electricity purchased from the main grid. Additionally, using the dynamic rating of the lines in small grids allows for connection of additional consumers with lesser need in additional investment compared to the standard scenario. Dynamic rating does not only reduce the investment cost in new DERs, when planning microgrids, but creates a possibility of facilitating increasing power demand in the future.

Overall, applying dynamic rating to lines in microgrids has high potential. However, it has to be noted that risks and reliability impacts of using DLR in low and medium voltage grids have to be additionally evaluated. Additionally, time horizon aspects can be included in the problem for improving the design and having optimal schedule for investing in additional energy sources.

Acknowledgment

The authors would like to thank Ola Ivarsson and Claes Ahlrot from E.ON. Energidistribution AB and Tor Laneryd from Hitachi ABB Power Grids for providing feedback and guidance for the project.

This project is conducted under STandUP for Wind framework.

References

[1] B. Xu, A. Ulbig, and G. Andersson, "Impacts of dynamic line rating on power dispatch performance and grid integration of renewable energy sources," in *Proc. IEEE PES ISGT Eur.*, Lyngby, Denmark, Oct. 2013, pp. 1–5.

[2] N. Viafora, S. Delikaraoglou, P. Pinson, and J. Holbøll, "Chance-constrained optimal power flow with non-parametric probability distributions of dynamic line ratings," *Int. J. Elect. Power Energy Syst.*, vol. 114, Jan. 2020, Art. no. 105389. [Online]. Available: http://www.sciencedirect.com/science/article/pii/S0142061519309317

[3] N. Viafora, "Optimized utilization of transmission grid capacity—Dynamic rating versus grid performance," Ph.D. dissertation, Dept. Elect. Eng., Techn. Univ. Denmark, Kongens Lyngby, Denmark, 2020.

[4] K. Morozovska, W. Naim, N. Viafora, E. Shayesteh, and P. Hilber, "A framework for application of dynamic line rating to aluminum conductor steel reinforced cables based on mechanical strength and durability," *Int. J. Elect. Power Energy Syst.*, vol. 116, Mar. 2020, Art. no. 105491. [Online]. Available: http://www.sciencedirect.com/science/article/pii/S0142061519309494

[5] K. W. Cheung and J. Wu, "Incorporating dynamic line ratings in real-time dispatch of market and system operations," in *Proc. IEEE Power Energy Soc. General Meeting (PESGM)*, Boston, MA, USA, Jul. 2016, pp. 1–5.

[6] F. Teng, R. Dupin, A. Michiorri, G. Kariniotakis, Y. Chen, and G. Strbac, "Understanding the benefits of dynamic line rating under multiple sources of uncertainty," *IEEE Trans. Power Syst.*, vol. 33, no. 3, pp. 3306–3314, May 2018.

[7] M. Tschampion, M. A. Bucher, A. Ulbig, and G. Andersson, "N-1 security assessment incorporating the flexibility offered by dynamic line rating," in *Proc. Power Syst. Comput. Conf. (PSCC)*, Genoa, Italy, Jun. 2016, pp. 1–7.

[8] N. Viafora, K. Morozovska, S. H. H. Kazmi, T. Laneryd, P. Hilber, and J. Holbøll, "Day-ahead dispatch optimization with dynamic thermal rating of transformers and overhead lines," *Elect. Power Syst. Res.*, vol. 171, pp. 194–208, 2019. [Online]. Available: http://www.sciencedirect.com/science/article/pii/S0378779619300902

[9] M. Dabbaghjamanesh, A. Kavousi-Fard, and S. Mehraeen, "Effective scheduling of reconfigurable microgrids with dynamic thermal line rating," *IEEE Trans. Ind. Electron.*, vol. 66, no. 2, pp. 1552–1564, Feb. 2019.

[10] S. Mashayekh, M. Stadler, G. Cardoso, and M. Heleno, "A mixed integer linear programming approach for optimal DER portfolio, sizing, and placement in multi-energy microgrids," *Appl. Energy*, vol. 187, pp. 154–168, Feb. 2017. [Online]. Available: http://www.sciencedirect.com/science/article/pii/S0306261916316051

[11] S. Mashayekh *et al.*, "Security-constrained design of isolated multi-energy microgrids," *IEEE Trans. Power Syst.*, vol. 33, no. 3, pp. 2452–2462, May 2018.

[12] M. R. Vallem and J. Mitra, "Siting and sizing of distributed generation for optimal microgrid architecture," in *Proc. 37th Annu. North Amer. Power Symp.*, Ames, IA, USA, Oct. 2005, pp. 611–616.

[13] M. R. Vallem, J. Mitra, and S. B. Patra, "Distributed generation placement for optimal microgrid architecture," in *Proc. IEEE/PES Transm. Distrib. Conf. Exhibit.*, Dallas, TX, USA, May 2006, pp. 1191–1195.

[14] *IEEE Standard for Calculating the Current-Temperature Relationship of Bare Overhead Conductors*, IEEE Standard Std 738-2012, pp. 1–72, Dec. 2013.

[15] J. Iglesias *et al.*, "Guide for thermal rating calculation of overhead lines," in *CIGRE Working Group B2.43*, CIGRE, Paris, France, 2014, p. 93.

[16] D. Roberts, P. Taylor, and A. Michiorri, "Dynamic thermal rating for increasing network capacity and delaying network reinforcements," in *Proc. SmartGrids Distrib. IET-CIRED Seminar*, 2008, pp. 1–4.

[17] A. Michiorri *et al.*, "Forecasting for dynamic line rating," *Renew. Sustain. Energy Rev.*, vol. 52, pp. 1713–1730, Dec. 2015. [Online]. Available: http://www.sciencedirect.com/science/article/pii/S1364032115007819

[18] S. Talpur, C. Wallnerstrom, C. Flood, and P. Hilber, "Implementation of dynamic line rating in a sub-transmission system for wind power integration," *Smart Grid Renew. Energy*, vol. 6, no. 8, pp. 233–249, Aug. 2015.

[19] K. Morozovska and P. Hilber, "Study of the monitoring systems for dynamic line rating," in *Proc. 8th Int. Conf. Appl. Energy*, Oct. 2016, pp. 1–6.

[20] J. F. Franco, M. J. Rider, M. Lavorato, and R. Romero, "A mixed-integer LP model for the reconfiguration of radial electric distribution systems considering distributed generation," *Elect. Power Syst. Res.*, vol. 97, pp. 51–60, Apr. 2013. [Online]. Available: http://www.sciencedirect.com/science/article/pii/S0378779612003574

[21] S. Wilcox and W. Marion, "Users manual for TMY3 data sets," NREL, Golden, CO, USA, Rep. NREL/TP-581-43156, May 2008.

[22] M. Deru *et al.*, "U.S. department of energy commercial reference building models of the national building stock," NREL, Golden, CO, USA, Rep. NREL/TP-5500-46861, Feb. 2011.

[23] P. Larsson and P. Börjesson, "Cost models for battery energy storage systems," Ph.D. dissertation, Dept. Bachelor Sci., KTH School Ind. Eng. Manage., Stockholm, Sweden, 2018.

[24] Energy Sage. (2018). *How Much Do Solar Panels Cost in the U.S. in 2019?* [Online]. Available: https://news.energysage.com/how-much-does-the-average-solar-panel-installation-cost-in-the-u-s/

[25] EIA Independent Statistics & Analysis. U.S. Energy Information Administration. (2019). *Electricity Monthly Update. Regional Wholesale Markets: July 2019*. [Online]. Available: https://www.eia.gov/electricity/monthly/update/wholesale_markets.php

[26] Gurobi Optimization, LLC. (2019). *Gurobi Optimizer Reference Manual*. [Online]. Available: http://www.gurobi.com